NASA/TM—2014-218372

Experimental and Theoretical Study of Thermodynamics of the Reaction of Titania and Water at High Temperatures

QuynhGiao N. Nguyen
Glenn Research Center, Cleveland, Ohio

Dwight L. Myers
East Central University, Ada, Oklahoma

Nathan S. Jacobson
Glenn Research Center, Cleveland, Ohio

Elizabeth J. Opila
University of Virginia, Charlottesville, Virginia

October 2014

NASA STI Program . . . in Profile

Since its founding, NASA has been dedicated to the advancement of aeronautics and space science. The NASA Scientific and Technical Information (STI) program plays a key part in helping NASA maintain this important role.

The NASA STI Program operates under the auspices of the Agency Chief Information Officer. It collects, organizes, provides for archiving, and disseminates NASA's STI. The NASA STI program provides access to the NASA Aeronautics and Space Database and its public interface, the NASA Technical Reports Server, thus providing one of the largest collections of aeronautical and space science STI in the world. Results are published in both non-NASA channels and by NASA in the NASA STI Report Series, which includes the following report types:

- TECHNICAL PUBLICATION. Reports of completed research or a major significant phase of research that present the results of NASA programs and include extensive data or theoretical analysis. Includes compilations of significant scientific and technical data and information deemed to be of continuing reference value. NASA counterpart of peer-reviewed formal professional papers but has less stringent limitations on manuscript length and extent of graphic presentations.

- TECHNICAL MEMORANDUM. Scientific and technical findings that are preliminary or of specialized interest, e.g., quick release reports, working papers, and bibliographies that contain minimal annotation. Does not contain extensive analysis.

- CONTRACTOR REPORT. Scientific and technical findings by NASA-sponsored contractors and grantees.

- CONFERENCE PUBLICATION. Collected papers from scientific and technical conferences, symposia, seminars, or other meetings sponsored or cosponsored by NASA.

- SPECIAL PUBLICATION. Scientific, technical, or historical information from NASA programs, projects, and missions, often concerned with subjects having substantial public interest.

- TECHNICAL TRANSLATION. English-language translations of foreign scientific and technical material pertinent to NASA's mission.

Specialized services also include creating custom thesauri, building customized databases, organizing and publishing research results.

For more information about the NASA STI program, see the following:

- Access the NASA STI program home page at *http://www.sti.nasa.gov*

- E-mail your question to *help@sti.nasa.gov*

- Fax your question to the NASA STI Information Desk at 443–757–5803

- Phone the NASA STI Information Desk at 443–757–5802

- Write to:
  STI Information Desk
  NASA Center for AeroSpace Information
  7115 Standard Drive
  Hanover, MD 21076–1320

NASA/TM—2014-218372

Experimental and Theoretical Study of Thermodynamics of the Reaction of Titania and Water at High Temperatures

QuynhGiao N. Nguyen
Glenn Research Center, Cleveland, Ohio

Dwight L. Myers
East Central University, Ada, Oklahoma

Nathan S. Jacobson
Glenn Research Center, Cleveland, Ohio

Elizabeth J. Opila
University of Virginia, Charlottesville, Virginia

National Aeronautics and
Space Administration

Glenn Research Center
Cleveland, Ohio 44135

October 2014

Acknowledgments

This work represents in part the Ph.D. dissertation (Q. Nguyen) in Chemistry from Cleveland State University. Thanks to D. Johnson, from NASA Glenn Research Center (GRC), for analytical lab analyses and D. Humphrey from ZIN Technologies, Inc., for experimental assistance with the furnace set-up and maintenance. This work was supported by the NASA Glenn Independent Research & Development program. Much of the computing for this project was performed at the Oklahoma Supercomputing Center for Education and Research (OSCER) at the University of Oklahoma (OU). OSCER Director Henry Neeman, David Akin, Senior System Administrator, and Joshua Alexander, HPC Application Software Specialist all provided valuable technical advice.

Level of Review: This material has been technically reviewed by technical management.

Available from

NASA Center for Aerospace Information
7115 Standard Drive
Hanover, MD 21076–1320

National Technical Information Service
5301 Shawnee Road
Alexandria, VA 22312

Available electronically at http://www.sti.nasa.gov

Experimental and Theoretical Study of Thermodynamics of the Reaction of Titania and Water at High Temperatures

QuynhGiao N. Nguyen
National Aeronautics and Space Administration
Glenn Research Center
Cleveland, Ohio 44135

Dwight L. Myers
East Central University
Ada, Oklahoma 74820

Nathan S. Jacobson
National Aeronautics and Space Administration
Glenn Research Center
Cleveland, Ohio 44135

Elizabeth J. Opila
University of Virginia
Charlottesville, Virginia 22904

Abstract

The transpiration method was used to determine the volatility of titanium dioxide (TiO_2) in water vapor-containing environments at temperatures between 1473 and 1673 K. Water contents ranged from 0 to 76 mole % in oxygen or argon carrier gases for 20 to 250 hr exposure times. Results indicate that oxygen is not a key contributor to volatilization and the primary reaction for volatilization in this temperature range is: $TiO_2(s) + H_2O(g) = TiO(OH)_2(g)$. Data were analyzed with both the second and third law methods to extract an enthalpy and entropy of formation. The geometry and vibrational frequencies of $TiO(OH)_2(g)$ were computed using B3LYP density functional theory, and the enthalpy of formation was computed using the coupled-cluster singles and doubles method with a perturbative correction for connected triple substitutions [CCSD(T)]. Thermal functions are calculated using both a structure with bent and linear hydroxyl groups. Calculated second and third heats show closer agreement with the linear hydroxyl group, suggesting more experimental and computational spectroscopic and structural work is needed on this system.

Introduction

Many common oxides react with water vapor at high temperatures to form hydroxide and oxyhydroxide species (Refs. 1 and 2). Precise thermodynamic data are available for some of these species such as the Group I and Group II hydroxides (Ref. 3), $Si(OH)_4(g)$ (Refs. 4 to 6) and $CrO_2(OH)_2(g)$ (Ref. 7). However, data are unavailable for many important hydroxides and oxyhydroxides.

Titania-forming and titania-containing materials are of great interest for applications in high temperature environments due to their temperature capabilities, light weight, good strength-to-weight ratio and corrosion resistance. Examples include Ti(Pt)Ni nitinol, Ti-Al alloys, TiB_2, TiN, TiC, and refractory coatings containing TiO_2. Since high temperature combustion environments contain water vapor, the interaction of water vapor and titania is important. In addition, such processes are important in geological phenomena. However we could find no thermodynamic data for titanium hydroxides or oxyhydroxides. Further, the exact stoichiometry of the titanium hydroxide or oxyhydroxide species is not known.

There is laboratory evidence that TiO_2 does indeed react with water vapor. Several groups have conducted matrix isolation experiments and obtained infrared spectra of species condensed on an Ar

matrix. Most of the studies examine the interaction of Ti metal atoms with H_2O. Kauffman et al. (Ref. 8) see evidence for $H_xTi(OH)_2$ and $Ti(OH)_x$. Zhou et al. (Ref. 9) suggest $H_2Ti(OH)_2$. Wang and Andrews (Ref. 10) see evidence of $Ti(OH)_2$ and $Ti(OH)_4$. Shao et al. (Ref. 11) examined TiO_2 interactions with H_2O and report on the structure and vibrational frequencies of $OTi(OH)_2$. At high temperatures, Ueno and colleagues reported evidence of attack of rutile in a 30 mass percent H_2O/Air environment at 1773 K (Ref. 12) in the form of weight loss and etch pits. They also discuss the reaction of TiO_2 in hot water, which is attributed to the formation of $Ti(OH)_4$ (Ref. 13).

A generalized reaction for TiO_2(s) with oxygen and water vapor is:

$$TiO_2(s) + xO_2(g) + yH_2O(g) = TiO_{(2+2x+y)}H_{(2y)}\,(g) \tag{1}$$

Thus $P(TiO_{(2+2x+y)}H_{(2y)})$ varies with $[P(O_2)]^x$ and $[P(H_2O)]^y$. In our laboratories and others, the transpiration method has been found to be particularly useful for the study of this type of reaction at elevated temperatures (Refs. 5, 7, 14, and 15). The transpiration method as reviewed by Merton and Bell (Ref. 16), involves flowing reactant gases over a condensed sample at a suitable rate in order for solid-gas equilibrium to be established. The product gas flows downstream and is condensed in a cooler portion of the gas train, collected and analyzed to quantitatively determine the amount of sample transported. By independently varying the reactant gas partial pressures and determining the dependence of volatile product formation on reactant gas concentration, the identity of volatile species can be determined. The partial pressure of the volatile species, $TiO_{(2+2x+y)}H_{(2y)}$ (g), can then be determined over a range of temperatures, which allows the extraction of an enthalpy and entropy of reaction.

In this study we supplement these experimental measurements with computational studies. The goal of this study is to utilize both approaches to determine the thermodynamics of the TiO_2 and H_2O interactions at elevated temperatures.

Experimental Procedure

TiO_2 Pellets

Acros Organics, 99.999 percent pure titanium oxide, predominately rutile, powder was cold-pressed in a 1/4 in. O.D. stainless steel die to a pressure of 141 kg/cm^2 (2000 psig). These pellets were dried overnight in a 100 °C drying oven and were sintered in air at 1200 °C for 24 hr. The TiO_2 pellets were weighed and the density was calculated to be 3.75 g/cc, corresponding to 88 percent of the theoretical density.

After the transpiration runs were complete, the reaction chamber was opened and the pellets were examined with x-ray diffraction and scanning electron microscopy. No significant changes in composition were noted. Typical surface morphologies of the pellets before and after exposure are shown in Figure 1. The grains were still rutile, as confirmed by x-ray diffraction, but significant grain growth occurred.

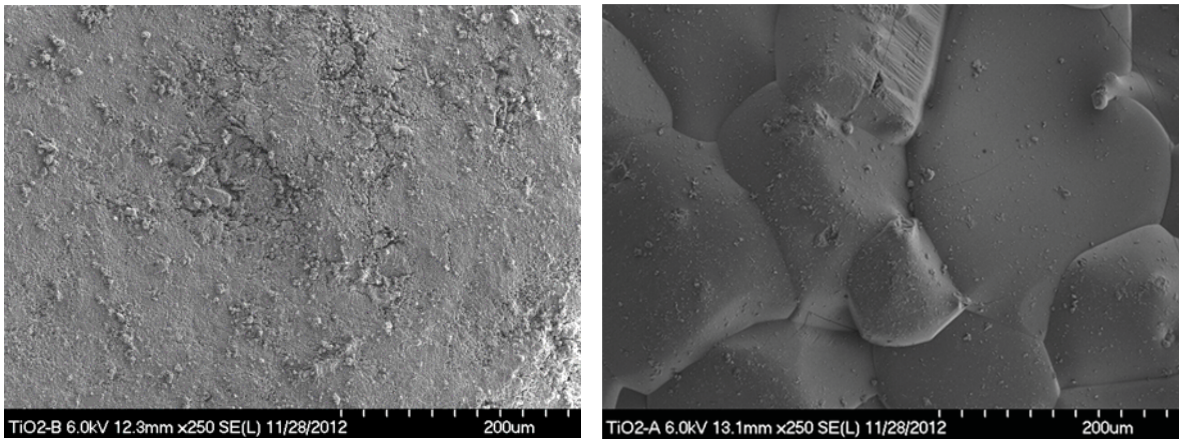

Figure 1.—View of starting pellet. (a) Before the transpiration experiments. (b) After the transpiration experiments, showing the extensive grain growth.

Transpiration System

The transpiration system is shown schematically in Figure 2. The cell is made out of platinum-20 percent rhodium, (Pt/20Rh), and laser welded with the sintered TiO_2 pellets packed inside. A type R thermocouple is inserted through the bottom of the cell to monitor the reaction temperature. A carrier gas composed of argon and/or oxygen flowed through the reaction cell and was controlled and monitored with a calibrated electronic flowmeter (Tylan FC-260).

Furnace Set-Up

The transpiration system used a furnace with molydisilicide heating elements (Applied Test Systems, Inc.) and a 99.8 percent pure alumina furnace tube. Deionized water was introduced through the bottom of the transpiration gas train into the carrier gas via a peristaltic pump. The liquid water flow rate ranged from 0.5 to 9.3 ml/hr and was calibrated before and after each test to verify the flow consistency. A quartz wool plug, located at the junction of the water inlet with the gas train, was used to ensure that liquid to vapor disbursement occurred. The gases (Ar, O_2, and water vapor) were introduced through the bottom of the transpiration gas train and then flowed into the transpiration cell. The flow rates of the gases (argon/oxygen) ranged from 60 to 275 cc/min. Whenever the furnace was above room temperature, the blanket Ar gas that flows on the exterior of the transpiration cell was flowing at rates of 90 cc/min or higher. The gas lines and water line were heated with heating tape (260 °C) prior to introduction into the furnace. This prevented condensation and provided some pre-heating of the gas. The gas stream traveled up through the sealed reaction chamber, located in the hot zone of the furnace, and then exited through a series of three fused quartz (99.995 percent purity) condensation (collection) tubes, as shown in red on Figure 2.

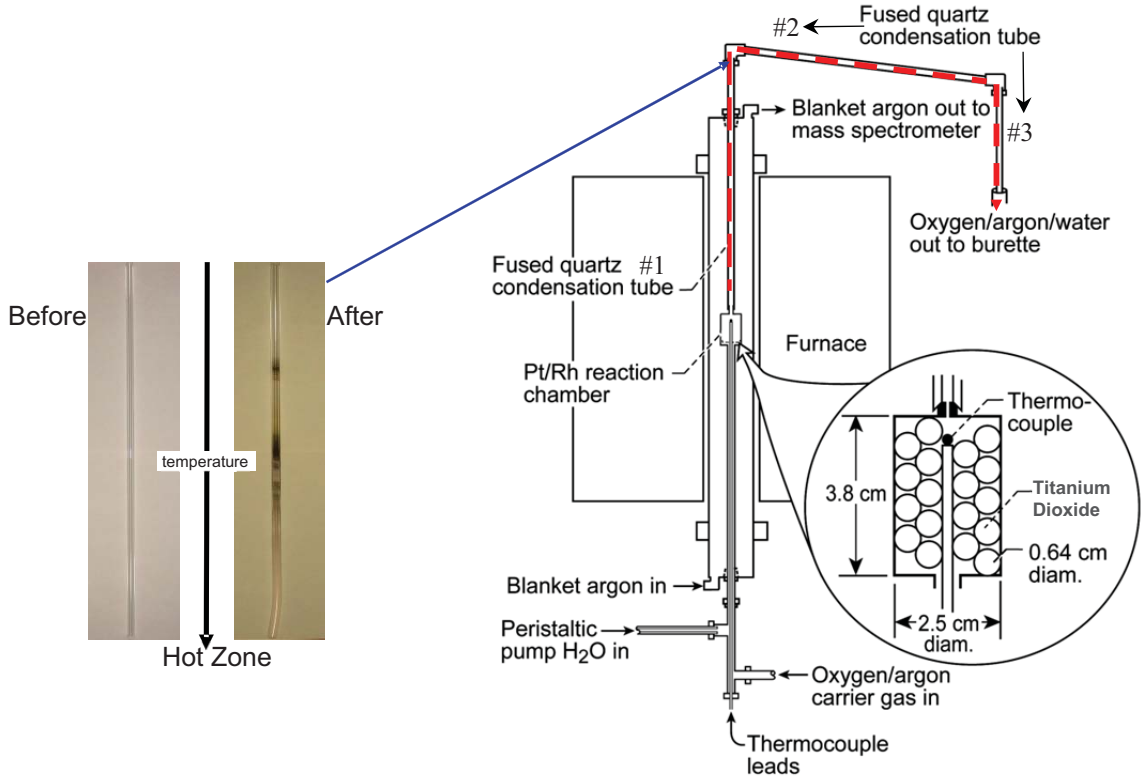

Figure 2.—Transpiration furnace and transpiration cell (Pt/Rh Reaction Chamber). The insets show the details of the reaction chamber and condensate on the quartz collection tubes.

From our previous studies on the Cr-O-H system (Ref. 7), it was found to be critical to analyze all the deposits in the entire gas train after the reaction chamber. The series of three fused quartz condensation tubes was held together by polyfluoroethylene fittings. The first condensation tube (#1), as mentioned above was located in the hot zone at the exit of the transpiration cell in the center of the furnace. This condensation tube will be referred to as the main straight condensation tube where the primary condensate was collected. The end that sat in the hot zone of the furnace had an internal beveled edge that snuggly fit over the transpiration cell exit, thus allowing for a tight seal and maintaining pressure as the gases exited. This straight condensation tube was replaced after each experiment due to the devitrification and resultant damage that occurs during cooling from the high temperature exposures. An image of this tube is shown in the inset in Figure 2. The second fused quartz condensation tube (#2) was a bent one located at the top of the furnace tube. This second fused quartz condensation tube was wrapped with heating tape to ensure the water vapor did not condense prior to reaching the third condensation tube (#3). The third tube was at room temperature, thus allowing the water vapor to condense, collect in a buret, and be measured. Both the second and third fused quartz condensation tubes were reused after the Ti-deposits had been extracted by an analytical method explained in the next section. All the fused quartz tubes and polyfluoroethylene fittings were kept in a clean drying oven held at 100 °C to eliminate any moisture when not in use for an experiment. The experiments were conducted at ambient pressure. The transpiration cell pressure was recorded with a capacitance manometer (Leybold Inficon) that varied between 0.96 to 1.00 atm (730 to 763 Torr) during the two years of testing. This capacitance monitor was verified by a separate barometric standard (NASA Glenn Aircraft Hanger Barometer, http://barometer.grc.nasa.gov/cgi-bin/barometer.cgi). To verify that there were no leaks in the system, the pressure was checked for each experiment by closing the exhaust and watching the back pressure increase as measured by the capacitance manometer.

Chemical Analyses

The amount of Ti condensate in the three fused quartz condensation tubes along with the polyfluoroethylene fittings and water that was collected through the exhaust was quantitatively analyzed using inductively coupled plasma atomic emission spectroscopy (ICP-AES) (Varian Vista-Pro, Axial configuration). The fittings and exhaust waters contained no visible deposits. The fittings were digested in a 5 percent (by volume) hydrochloric acid (HCl) + 2 percent hydrofluoric acid (HF) solution for 2 to 3 hr. This solution and the exhaust water were diluted to a known volume and ICP-AES was used to measure the Ti concentration. The absence of deposit in the exhaust water was also verified in the first several runs by a filtration step resulting in no weight change on Whatman grade #44 filter paper (nominal particle retention size > 3 μm, filtration speed, slow).

The inside of the main straight fused quartz condensation tube #1 (which includes the hot zone) contained a film on the internal walls in the form of a brown to black deposit. This main condensation tube acquired the most Ti-deposit relative to the other tubes, although some deposit was also formed in the internal walls of tube #2. The fused quartz tubes were soaked in an aqua regia solution (3 parts HCl + 1 part nitric acid (HNO_3)) for 2 hr followed by a rinse with concentrated HF. Based on the analysis of the first several runs that contained only Ar(g) and H_2O(g), the black deposits collected from the aqua regia soak were filtered and discarded, since they contained no Ti deposits. This was confirmed with wavelength dispersive x-ray fluorescence (WDXRF). The runs exposed to oxygen formed reaction products from the TiO_2 pellets but also from the Pt/Rh reaction chamber. The latter was a black deposit, likely platinum oxide (PtO) as indicated by WDXRF, that was strongly bonded to the Ti-condensate. All runs that contained oxygen went through a second series of analysis in which an acidic flux (fusion) step through the use of potassium hydrogen sulfate (pyrosulfate) was used in order to extract the Ti-condensate. This mixture was heated over a Bunsen burner until it liquefied, thus converting any remaining TiO_2(s) into a soluble solution that can be analyzed in the ICP-AES.

The presence of a black deposit was a concern. The first several runs' black deposits (PtO) were filtered and dried after the acidic flux (fusion) extraction and characterized by WDXRF to confirm the absence of Ti. The typical weight of these black deposits was estimated to be 10 to 20 mg. Since the

WDXRD sensitivity to Ti is typically about 0.1 percent (Ref. 17), it is possible that up to 20 μg still remained in this deposit. Several additional methods were tried to dissolve the black deposits. These include successive aqua regia and concentrated HF exposures; a flux of sodium carbonate and sodium tetraborate; and a flux of boric acid and sodium fluoride. The black deposit was not significantly attacked. The resultant solution from the acid dissolution contained only 1 μg Ti. The potential for trace concentrations of Ti in the black deposit must be considered a possible source of error. However, black deposits were not formed in experiments run with only argon gas and hence more confidence is given to data from these runs.

The second and third quartz condensation tubes along with all the polyfluorethylene fittings were reused since they were not exposed to high temperatures. The third tube and fittings went through a series of acid soaks, which involved an overnight soak in 50 percent solution of HCl followed by a deionized water rinse, drying and were stored in a clean drying oven (100 °C) prior to reuse.

It is also important to note that the ICP-AES procedure is very sensitive for measuring cations and can detect to several micrograms, as found in previous studies (Refs. 5 and 7). The amount of Ti in the condensate ranged between 9 and 262 μg.

Calculations With Experimental Data to Identify the Species and Extract Thermodynamic Data

The identity of the volatile species was determined by using the measured data to calculate the coefficients x and y in reaction (1). The same calculation methods were used in previous studies (Refs. 5 and 7). The vapor pressure of the volatile Ti-O-H species, $P_{Ti\text{-}O\text{-}H}$, is given by:

$$P_{Ti-O-H} = \frac{\dot{n}_{Ti} R T_{cell}}{\dot{V}} \tag{2}$$

Here $\dot{n}_{Ti}$ is the molar rate of Ti from the reaction cell, R is the ideal gas constant, T_{cell} is the measured temperature inside the cell, and $\dot{V}$ is the total volumetric flow rate through the reaction cell. The molar flow rate of Ti is simply the rate at which Ti is deposited downstream:

$$\dot{n}_{Ti} = \frac{m_{Ti}}{M_{Ti} t} \tag{3}$$

Here m_{Ti} is the mass of Ti collected at the end of an experiment, M_{Ti} is the atomic weight of Ti, and t is duration of an experiment. The total flow rate through the cell is simply the sum of all the flow rates through the cell:

$$\dot{V} = \frac{R T_{cell}}{P_{tot}} \left(\dot{n}_{O_2} + \dot{n}_{Ar} + \dot{n}_{H_2O} + \dot{n}_{Ti-O-H} \right) \tag{4}$$

Here P_{tot} is the total pressure. The last quantity in Equation (4), $\dot{n}_{Ti-O-H}$, is the same as $\dot{n}_{Ti}$ and is much smaller than the others. It can thus be neglected. Note also that these flow rates are all at 298.15 K.

Initially a series of experiments was conducted to identify the product of the reaction of TiO_2 and O_2/H_2O. This was done by systematically varying P_{O_2} and P_{H_2O}. Once the molecule was identified, vapor pressures were determined. Second and third law methods were then used to derive thermodynamic parameters (Ref. 18). The second law method gives a heat of reaction, $\Delta_r H^{o}_{T_{av}}$, at the average temperature of measurement, $T_{av,}$ using the van't Hoff equation.

$$\frac{d\left(\ln K_p\right)}{d\left(\frac{1}{T}\right)} = -\frac{\Delta_r H^o_{T\,av}}{R} \tag{5}$$

Here K_p is the equilibrium constant for reaction (1) with known x and y and R is the gas constant. In order to obtain a heat of reaction at 298.15 K, the following expression is used:

$$\Delta_r H^o_T = \Delta_r H^o_{298} + \int_{298}^{T} \Delta C_p \, dT \tag{6}$$

The Gibbs energy function (*gef*) is given by

$$gef_{298.15} = \left(G^o_T - H^o_{298.15}\right)/T \tag{7}$$

The standard entropy, heat capacity, and Gibbs energy function were all calculated from the statistical mechanics methods, using calculated vibrational frequencies (Ref. 19). If good Gibbs energy functions are determined, the third law method (Ref. 18) can be used to derive the enthalpy at 298.15 K, using Equation (8) for each data point.

$$T\left\{\Delta\left\{-\left(gef_{298.15}\right)\right\} - R\ln\left(P_{Ti-O-H}\right)\right\} = \Delta_{rxn}\, H^o_{298.15}\left(Ti - O - H\right) \tag{8}$$

Results

Identity of the Ti-O-H Species

A total of 51 tests were conducted over a temperature range of 1473 to 1673 K and are listed in Appendix A. This study was conducted for three primary temperatures of interest: 1473, 1573, and 1673 K along with additional measurements at 1498, 1523, and 1548 K. As discussed in the experimental section, the identity of the major Ti-O-H species is determined by methodically varying the O_2 and H_2O reactants.

First consider the measurements at 1673 K to determine the value of x and y in Equation (1), as shown in Figure 3. At the highest temperature, the amount of Ti collected was the largest, leading to less scatter in the data.

A similar analysis was applied to the data at 1573 K. At this temperature, when the H_2O content was held at 24 percent and the O_2 content was varied the value of x is 0.07±0.01; when O_2 content was held at 34 percent and the H_2O content is varied the value of y was 0.85±0.09. At constant $P(H_2O)$, variation in $P(O_2)$ does not change the amount of Ti-O-H(g) formation suggesting the coefficient, x in reaction (1) is zero. At constant $P(O_2)$, the amount of Ti-O-H(g) formation varies with $[P(H_2O)]^1$, suggesting the coefficient, y in reaction (1) is one. Thus results at 1573 and 1673 K suggest the primary reaction is:

$$TiO_2(s) + H_2O(g) = TiO(OH)_2(g) \tag{9}$$

Figure 4 is a plot of all the data versus $P(H_2O)$. Note the slopes are all close to one, confirming the stoichiometry of reaction (9). The data obtained at 1473 K show a larger amount of scatter due to the very small amount of downstream deposit collected.

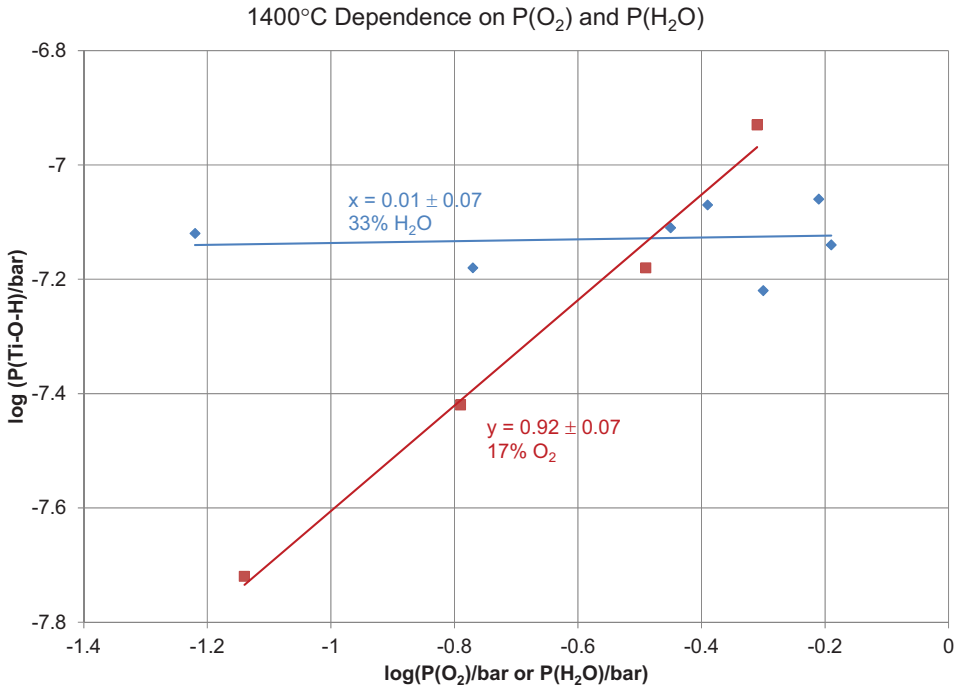

Figure 3.—Measured partial pressure of Ti-O-H at 1673 K. O_2(g) or H_2O(g) is held constant at the values indicated.

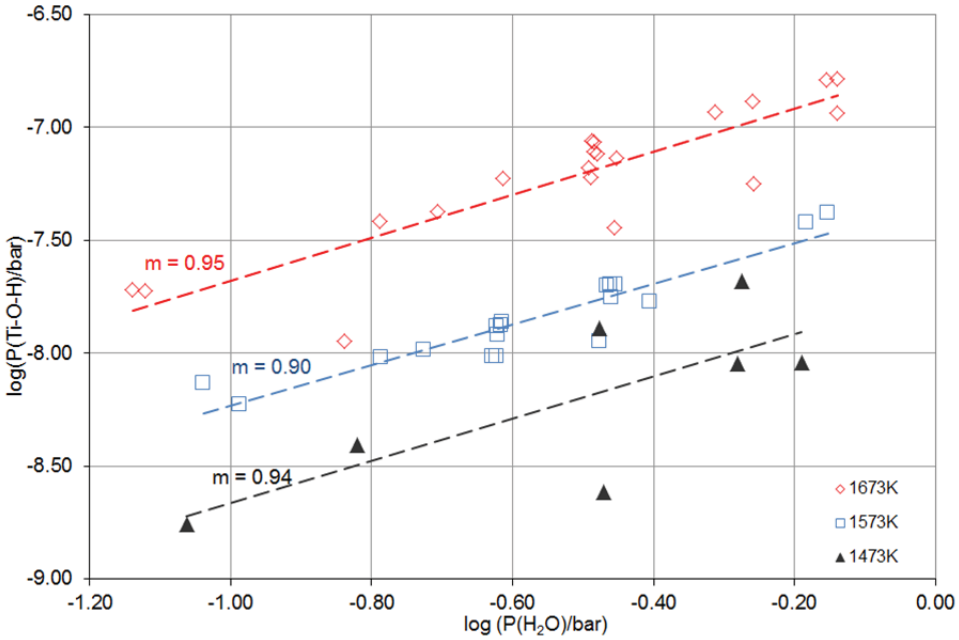

Figure 4.—Vapor pressure as a function of $P(H_2O)$ for 1473, 1573, and 1673 K.

Derivation of the Gibbs Energy Function for $TiO(OH)_2(g)$

Shao et al. (Ref. 11) have conducted infrared (IR) matrix isolation spectroscopy on the products of $TiO_2(s) + H_2O$ and observed $TiO(OH)_2$. They also conducted density-functional theory (DFT) calculations, which are in good agreement with their experimental results. This study by Shao et al. provides the necessary molecular parameters to calculate the Gibbs energy function. Figure 5 is their derived structure with angles, bond lengths and C_{2v} symmetry. Table I lists their calculated vibrational frequencies. In addition, we conducted an optimization and frequency calculation using the Gaussian 09 program, revision B.01 (Ref. 20), and the B3LYP density functional with the cc-pVTZ+d basis set. Our results are also listed in Table I. As can be seen, our calculated frequencies are close to those of Shao et al.

We also consider the alternate structure in Figure 5(b). We use the 0.96×10^{-9} cm bond length for the O-H bond. We assume the calculated vibrational frequencies are the same for both structures and calculate the thermal functions for both structures.

The standard equations from statistical mechanics were used to calculate the entropy ($S^o(298)$) and the Gibbs energy function (*gef*) (Ref. 19). Using the geometry in Figure 5, the moment of inertia was calculated to be 4.8346×10^{-114} cm^6/g^3 and the symmetry number is 2. The molecule is a singlet, so there is no electronic contribution. The structure in Figure 5(a) is expected to have hindered internal rotations and the structure in Figure 5(b) is not expected to have any internal rotations. First consider the structure in Figure 5(a). The partition function of each internal rotation is given by:

$$Q_f = \frac{2.7934}{n}\left(10^{38} I_r T\right)^{1/2} \tag{10}$$

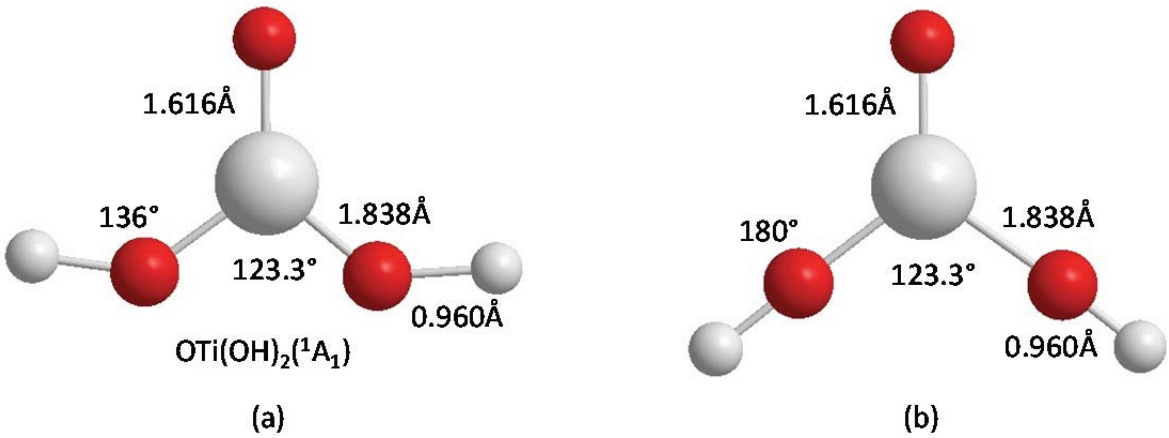

Figure 5.—(a) Structure of $TiO(OH)_2$ from (Ref. 11). (b) Alternate structure with linear –OH groups.

TABLE I.—VIBRATIONAL FREQUENCIES

Vibrational mode	Calculated frequency by DFT (Ref. 11), cm^{-1}	Calculated frequency (this study), cm^{-1}
a_1	3907.5	3885.2
b_2	3904.3	3882.1
a_1	1055.2	1082.7
b_2	784.3	805.3
a_1	678.6	700.2
b_1	537.8	529.1
a_2	515.1	511.7
b_2	474.0	510.3
a_1	460.1	509.0
b_2	225.0	234.9
a_1	192.8	201.0
b_1	53.3	49.1

Here I_r is the reduced moment of inertia for the –OH group, n is the symmetry number, and T is the absolute temperature. The reduced moment of inertia is defined by:

$$I_r = A\left(1 - \sum_{i=1}^{3} \frac{\alpha_i^2 A}{I_i}\right) \tag{11}$$

Here A is the moment of inertia of the –OH groups, α is the direct cosine of between the internal axis of rotation and the particular axis, and I_i is the moment about that axis. For this planar molecule there are only two direction cosines. The reduced moment of inertia is thus calculated to be 1.368×10^{-40} gm-cm^2. As in the case of $CrO_2(OH)_2$(g), two hindered internal rotors were assumed (Ref. 7). It is difficult to estimate the potential barrier to internal rotation, but we assume 12.6 kJ/mol (3 kcal/mol) here. Using the Tables of Pitzer and Gwinn (Ref. 21), the corrections for hindered rotations were determined. Given the predicted low potential barrier, the contribution from hindered internal rotations is not too much different than that for free internal rotations. Table II gives the contributions from the calculation for $S^o(298)$ for both structures.

The heat capacity can be determined from the standard statistical mechanics calculations (Ref. 20). These are listed in Table III(a) for the structure in Figure 5(a) and Table III(b) for the structure in Figure 5(b).

Table III(a) Heat capacities for $TiO(OH)_2$(g) structure 5(a). The total is obtained by summing the translational (2.5R) and rotational (1.5R), where R is the gas constant and the vibrational and hindered internal rotational contributions. Table III(b) Heat capacities for $TiO(OH)_2$(g) structure 5(b). The total is obtained by summing the translational (2.5R) and rotational (1.5R), where R is the gas constant and the vibrational and hindered internal rotational contributions.

TABLE II.—CALCULATION OF $S^O(298)$ FOR $TIO(OH)_2$(G)

Contribution	$S^o(298)$ J/mol-K Structure 5(a)	$S^o(298)$ J/mol-K Structure 5(b)
Translation	165.945	165.945
Rotation	100.42	100.589
Vibration	49.713	49.713
Hindered internal rotations (2)	27.872	----------
Total	343.95	316.247

TABLE III(a).—HEAT CAPACITIES FOR $TIO(OH)_2$(g) STRUCTURE 5(a)

Temperature, K	Vibrational	Two hindered rotations	Total C_p (J/mol-K)
300	51.428	37.579	122.263
400	61.290	36.582	131.127
500	67.530	36.582	137.367
600	71.656	35.750	140.663
700	74.595	34.919	142.769
800	76.872	34.919	145.047
900	78.773	34.919	146.948
1000	80.443	34.586	148.285
1100	81.952	34.420	149.628
1200	83.334	34.420	151.010
1300	84.603	34.254	152.112
1400	85.768	34.254	153.278
1500	86.836	34.087	154.179
1600	87.812	34.087	155.156

TABLE III(b).—HEAT CAPACITIES FOR
$TIO(OH)_2$(g) STRUCTURE 5(b)

Temperature, K	Vibrational	Total C_p (J/mol-K)
300	51.428	84.684
400	61.290	94.546
500	67.530	100.786
600	71.656	104.912
700	74.595	107.851
800	76.872	110.128
900	78.773	112.029
1000	80.443	113.699
1100	81.952	115.208
1200	83.334	116.590
1300	84.603	117.859
1400	85.768	119.024
1500	86.835	120.092
1600	87.812	121.068

The calculated Gibbs energy functions (*gef*) are similarly calculated, using the standard equation from statistical mechanics (Ref. 19). We converted the *gef* functions referenced to 0 K (*gef*0) to ones referenced to 298 K (*gef*298). In order to account for the hindered internal rotations, the tables in Pitzer and Gwinn (Ref. 21) were again used. In this case, we applied the following relations to the internal rotations:

$$gef\,0 = \left(\frac{G_T - H_o}{T}\right) = \left(\frac{H_T - TS_T - H_o}{T}\right) = \left(\frac{H_T - H_o}{T}\right) - S_T \tag{12}$$

Each of the quantities on the right side of Equation (10) is available in the tables of Pitzer and Gwinn (Ref. 21). Finally the correction to 298 K is given by:

$$gef\,298 = \left(\frac{G_T - H_o}{T}\right) - \left(\frac{H_{298} - H_o}{T}\right) \tag{13}$$

Table IV(a) and (b) gives the calculated Gibbs energy functions for the structures in Figure 5(a) and (b), respectively.

TABLE IV(a).—CALCULATED GIBBS ENERGY FUNCTIONS FOR THE STRUCTURE IN FIGURE 5(a)

T (K)	*gef*298 (translation)	*gef*298 (external rotation)	*gef*298 (vibrations)	*gef*298 (two internal rotations)	*gef*298 (total)
1400	–181.691	–109.891	–100.901	–38.636	–431.119
1500	–182.830	–110.575	–105.06	–39.576	–438.041
1600	–183.913	–111.225	–109.062	–40.417	–444.616
1700	–184.946	–111.844	–112.916	–41.244	–450.949

TABLE IV(b).—CALCULATED GIBBS ENERGY FUNCTIONS FOR
THE STRUCTURE IN FIGURE 5(b)

T (K)	*gef*298 (translation)	*gef*298 (external rotation)	*gef*298 (vibrations)	*gef*298 (total)
1400	–181.691	–110.691	–100.901	–392.652
1500	–182.830	–110.744	–105.06	–398.634
1600	–183.913	–111.394	–109.062	–404.37
1700	–184.875	–112.013	–112.916	–409.875

Data for TiO_2(s) and H_2O(g) were taken from the IVTAN tables (Ref. 22) to calculate the Δgef needed for the third law calculations in the next section.

Experimental Thermodynamic Data

A second law treatment of the data using a van't Hoff plot leads to an enthalpy and entropy of reaction at the average temperature of measurement (1600 K). This is shown in Figure 6.

Heat capacities are needed in order to obtain an enthalpy of reaction at 298.15 K. Equation (6) is applied for this and yields $\Delta_r H^o_{298} = 233.3 \pm 20$ kJ/mol with thermal functions for the structure in Figure 5(a) and $\Delta_r H^o_{298} = 251 \pm 20$ kJ/mol with thermal functions for the structure in Figure 5(b). Ideally the plot in Figure 6 could be used to extract an entropy, but we felt the scatter of the data was too great for a reliable number. Instead we take the calculated value in Table IV of $S^o_{298} = 343.95 \text{J/mol} - \text{K}$ with thermal functions for the structure in Figure 5(a) and $S^o_{298} = 316.247 \text{J/mol} - \text{K}$ with thermal functions for the structure in Figure 5(b). Finally the third law method was used to extract an enthalpy of reaction at 298 K, as described in the previous section. The value was $\Delta_r H^o_{298} = 403 \pm 13$ kJ/mol with thermal functions for the structure in Figure 5(a) and $\Delta_r H^o_{298} = 339 \pm 9$ kJ/mol with thermal functions for the structure in Figure 5(b). Clearly there is a large disparity regardless of which thermal functions are used, although the thermal functions for the structure in Figure 5(b) give somewhat closer results between the second and third law methods. The data are summarized in Table V. A similar disparity was found in our $CrO_2(OH)_2$(g) studies. These suggest that additional work is needed to determine the structure and develop the Gibbs energy functions for transition metal hydroxides.

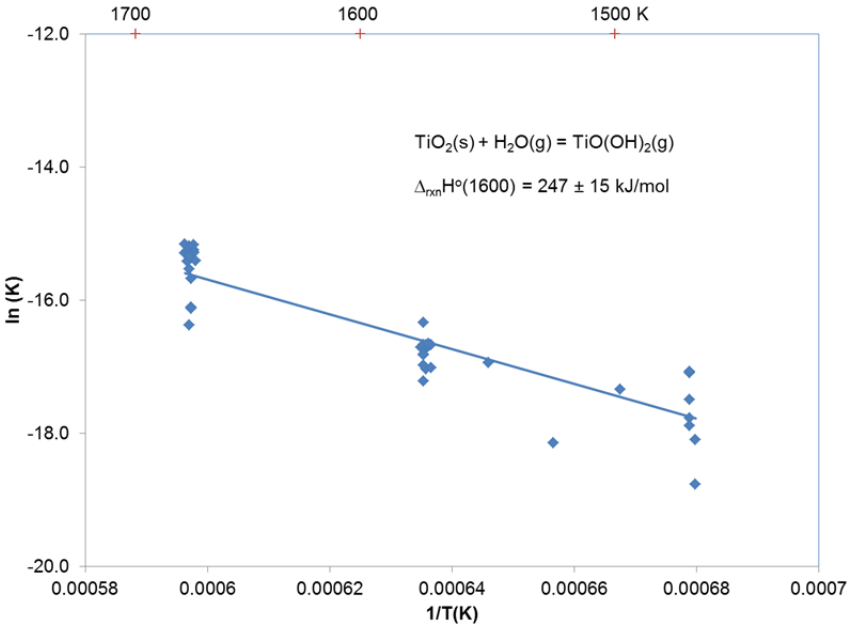

Figure 6.—Van't Hoff plot for the reaction of TiO_2(s) and H_2O(g).

TABLE V.—SUMMARY OF EXPERIMENTAL ENTALPIES OF REACTION

Method	$\Delta_f H^o_{298}$ (kJ/mol)	
	Thermal functions from Fig. 5(a)	Thermal functions from Fig. 5(b)
Second law	205±20	251±20
Third law	403±13	339±9

Computational Studies

In order to strengthen the experimental aspect of this study, some computational studies were conducted on the $TiO(OH)_2$ species. The Gaussian 09 program, revision B.01, was used for all calculations reported here (Ref. 21). A calculation of the enthalpy of formation of $TiO(OH)_2(g)$ was performed using a computational scheme which closely followed the technique employed previously by Opila et al. in computing the enthalpy of formation of $CrO_2(OH)_2(g)$ (Ref. 7). Geometries and harmonic vibrational frequencies for the participating species were computed using the B3LYP density functional method with the 6-311++G(d,p) basis set, which is of triple-ζ quality and includes diffuse and polarization functions on all atoms. The B3LYP/6-311++G(d,p) geometries and frequencies obtained were used for all subsequent energy calculations. In the reaction energy computations, electron correlation was accounted for by using a configuration interaction scheme with successive steps incorporating first coupled-cluster singles and doubles [CCSD], followed by a coupled-cluster singles and doubles method with a perturbative correction for connected triple substitutions [CCSD(T)]. For the coupled-cluster computations, the Bauschlicher Atomic Natural Orbital basis set (Ref. 23) was used for Ti, and for H and O the cc-pVTZ basis set was employed. Basis sets not available in the Gaussian Package were obtained from the Basis Set Exchange at the Environmental Molecular Science Laboratory at Pacific Northwest National Laboratory (Refs. 24 and 25).

The effect of inclusion of the titanium 3s and 3p core orbitals in the correlation procedure was computed using second-order Møller-Plesset perturbation (MP2) theory in conjunction with the cc-pVTZ basis for H and O and a modified Bauschlicher ANO set for Ti. The Bauschlicher ANO basis set was modified by decontracting the outermost six s, seven p, and seven d functions. A correction for basis-set incompleteness was estimated by computation of large-basis-set MP2 energies using a completely decontracted Bauschlicher ANO basis set on Ti and and the aug-cc-pVQZ set on H and O. Scalar relativistic effects were accounted for at the MP2 level using the Douglas-Kroll-Hess second-order relativistic correction. For Ti, the Bauschlicher ANO set, modified by decontracting the entire s and p spaces, was employed, and the cc-pVTZ_DK set was used for H and O. Temperature corrections $H°_{298.15} - H°_0$ for $TiO(OH)_2(g)$ were computed using the B3LYP/6-311++G(d,p) harmonic vibrational frequencies, employing standard formulas from statistical mechanics, and employing a free rotor treatment of the internal rotation of the hydroxide groups. These calculations were all done for the structure with the bent –OH group in Figure 5(b). However, the heat of formation should be similar, regardless of which structure these calculations are based on as the Ti-O skeleton dominates. Temperature corrections for $TiO_2(g)$ and $H_2O(g)$ were taken from the JANAF Tables. All computations for this method were performed at the OU Supercomputing Center for Education & Research (OSCER) at the University of Oklahoma (OU).

The heat of formation for $TiO(OH)_2(g)$ was computed using this scheme from the isogyric reaction:

$$TiO(OH)_2(g) \rightarrow TiO_2(g) + H_2O(g) \tag{14}$$

The reaction energy was first computed at 0 K and then converted to a reaction energy at 298.15 K by application of temperature corrections:

$$\Delta_r H^o_{298.15} = \Delta_r H^o_0 + H^o_{Thermal}(TiO_2) + H^o_{Thermal}(H_2O) - H^o_{Thermal}(TiO(OH)_2) \tag{15}$$

where $H^o_{Thermal} = H^o_{298.15} - H^o_0$. The heat of formation was then obtained from the expression:

$$\Delta_f H^o_T(TiO(OH)_2) = \Delta_f H^o_T(TiO_2) + \Delta_f H^o_T(H_2O) - \Delta_r H^o_T \tag{16}$$

TABLE VI.—COMPUTATION OF $\Delta_f H°_0$ AND $\Delta_f H°_{298}$ FOR $TiO(OH)_2$ FROM REACTION (14)

	Computational Increments	E/kJ mole^{-1}
	ΔE_e[HF]/kJ mol^{-1}	358.101
	∂[MP2]/kJ mol^{-1}	–115.812
	∂[CCSD]/kJ mol^{-1}	–264.317
	∂[CCSD(T)]/kJ mol^{-1}	224.920
	∂[core]/kJ mol^{-1}	+38.089
	∂[basis]/kJ mol^{-1}	+10.920
	∂[rel]/kJ mol^{-1}	–18.892
	∂[ZVPE]/kJ mol^{-1}	–5.177
	$\Delta_r H_0$ =	257.221 kJ mol^{-1}
	$\Delta_r H_{298}$ =	259.700 kJ mol^{-1}
Data source	IVTAN [22]	IVTAN [22]
T/K	298.15	0
$\Delta_f H°$ [H_2O]=	–241.826 kJ mol^{-1}	–238.921 kJ mol^{-1}
$\Delta_f H°$ [TiO_2]=	–322.856 kJ mol^{-1}	–320.000 kJ mol^{-1}
$\Delta_f H°$[$TiO(OH)_2$]=	–819.424 ± 49.856 kJ mol^{-1}	–816.142±49.856 kJ mol^{-1}

for $T = 0$ K and $T = 298.15$ K, using the literature values for the heats of formation of TiO_2(g) and H_2O(g) found in the literature (Ref. 23). The increments in the reaction energy are the changes in the computed energy in going from HF → MP2, MP2→CCSD, and CCSD→CCSD(T), and are designated as e.g., ∂[MP2], etc. In addition, the corrections for frozen core electrons, incompleteness of basis sets, and the relativistic correction were computed in subsequent steps. A correction for the zero-point vibrational energy was also computed. The energy increments, the calculated enthalpies of reaction, and the enthalpy of formation for $TiO(OH)_2$(g) as calculated using the composite method are given in Table VI. Errors are estimated for each correction and taken from the IVTAN reported tolerances for H_2O(g) and TiO_2(s) (Ref. 22). The deltas for the steps arriving at the final enthalpy of reaction were larger than for the same procedure as used by Opila, et al. (Ref. 7) in the computation of the enthalpy of formation of $CrO_2(OH)_2$(g). Therefore the error for this result is estimated as the square root of the squares of the normal expected precision in the method (Ref. 7) with the differences for the core, basis, and relativistic steps in the method added to the uncertainty, and including of course the published uncertainties in the enthalpies of formation for TiO_2(g) and H_2O(g).

Discussion

Clearly the determination of thermochemical data for $TiO(OH)_2$(g) is challenging both experimentally and theoretically. Experimentally the amount of material collected was very small and the insoluble black deposit could contain some Ti, resulting in uncertainty whether all the Ti was collected. Theoretically, composite quantum chemical methods are still developing for the transition metals.

Table VII compares the experimental and calculated enthalpies of formation and standard entropies. These quantities span a range of values and at this point we can only report a range of the enthalpy of formation. The thermal functions calculated for the structure in Figure 5(b) seem to give more consistent data.

Figure 7 shows a plot of experimental equilibrium constants as reported in Figure 6. We could not find any vapor pressure measurements of $TiO(OH)_2$(g) in the literature. However there are two studies of water-enhanced vaporization of TiO_2(s) (Refs. 12 and 26). It is possible to extract an approximate $P(TiO(OH)_2)$ and hence equilibrium constant from these studies. If we assume boundary layer limited flow the following expression relates partial pressure to vapor flux, *J,* for laminar flow (Ref. 27):

$$J = 0.664\left(\frac{\nu_\infty \rho_\infty L}{\eta}\right)^{0.5}\left(\frac{\eta}{D_i \rho_\infty}\right)^{0.33}\frac{D_i P_i}{\mathrm{R\,T}\,L} \tag{17a}$$

For turbulent flow this expression only changes slightly to (Ref. 28):

$$J = 0.0365\left(\frac{\nu_\infty \rho_\infty L}{\eta}\right)^{0.8}\left(\frac{\eta}{D_i \rho_\infty}\right)^{0.33}\frac{D_i P_i}{\mathrm{R\,T}\,L} \tag{17b}$$

Table VII gives the meaning of each of these variables and values for this estimation of vapor pressure from the studies of Ueno (Ref. 12) and Opila and Golden (Ref. 27).

Figure 7 compares the calculated equilibrium constant from this experimental/theoretical thermodynamic study to the two derived vapor pressures from the boundary layer limited vaporization studies. The boundary layer limited vaporization studies cannot be considered thermodynamic studies; however previous work has shown that equilibrium vapor pressures describe these processes (Refs. 31 and 32).

TABLE VII.—EXPERIMENTAL AND CALCULATED ENTHALPIES OF FORMATION AND STANDARD ENTHALPIES

	Method	$\Delta_f H^o_{298}$ (kJ/mol)		$S^o(298)$ (J/mol-K)	
		Thermal functions from Fig. 5(a)	Thermal functions from Fig. 5(b)	Thermal functions from Fig. 5(a)	Thermal functions from Fig. 5(b)
Experimental	Second law	–985±55	–934±55		
	Third law	–783±20	–847±20		
Theoretical	B3LYP DFT			353.95	316.247
	CCSD(T)	–820±50			

TABLE VIII.—VALUES TO ESTIMATE VAPOR PRESSURE FROM VAPOR FLUX DATA

Quantity	Value (Ueno)	Value (Opila and Golden)
Measured vapor flux, J	7.5×10^{-9} g/cm^2-s	1.209×10^{-7} g/cm^2-s
Free stream velocity, ν_∞	0.046 cm/s (Ref. 30)	1.75×10^{4} cm/s
Density of air: H_2O mixture, ρ_∞	1.239×10^{-4} g/cm^3	1.451×10^{-4} g/cm^3
Viscosity, η	6.014×10^{-4} g/cm-s (Ref. 30)	5.246×10^{-4} g/cm-s (Ref. 30)
Characteristic dimension, L	2.553 cm	1 cm
Gas phase diffusivity for $TiO(OH)_2$, D_i	2.046 cm^2/sec	1.544 cm^2/sec
Gas constant, R	82.06 cm^3-atm/mole-K	82.06 cm^3-atm/mole-K
Absolute temperature, T	1773 K	1513 K

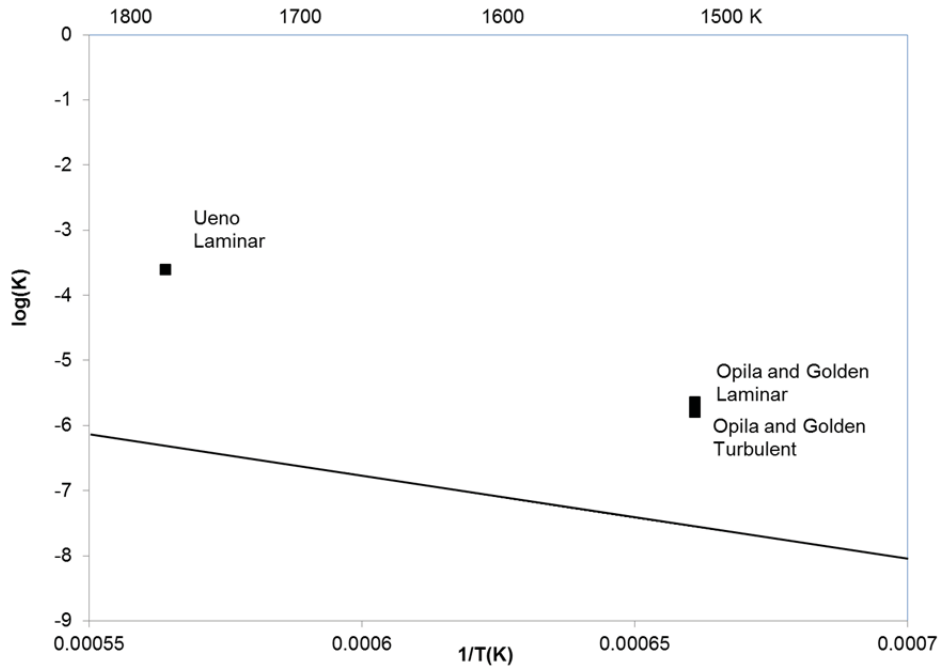

Figure 7.—Plot of pressure of $TiO(OH)_2(g)$ versus inverse temperature at $P(H_2O)$ = 1 bar, calculated using theoretically derived Gibbs energy functions and the third law experimental enthalpy above. The datapoints are extracted $P(TiO(OH)_2)$ from boundary layer limited vaporization studies.

Conclusions

The interaction of TiO_2 and $H_2O(g)/O_2(g)$ at temperatures from 1473 to 1673 K has been studied experimentally with the transpiration method and theoretically with quantum chemistry composite methods. Methodical variation of $P(H_2O)$ and $P(O_2)$ in transpiration studies identified the major product as $TiO(OH)_2(g)$. Experimental measurements were analyzed with both the second and third law methods. The geometry and vibrational frequencies of $TiO(OH)_2(g)$ were also computed using B3LYP density functional theory, and the enthalpy of formation was computed using the coupled-cluster singles and doubles method with a perturbative correction for connected triple substitutions [CCSD(T)]. Considerable spread was found between the second and third law enthalpy values. There appears to be some difficulty determining reliable Gibbs energy functions for this system, indicating a strong need for experimental and computational structure and spectroscopic studies. A comparison of the equilibrium constants from this experimental study to equilibrium constants extracted from studies of boundary layer limited vaporization showed some disparity. More studies are also needed to understand this.

Appendix A.—Raw Data

Run	Temp	Temp	Time	O_2 gas flow rate		Ar gas flow rate		H_2O flow rate		Room P_{total}	[Ti]	Condensate	Cell Flow rate	$P_{Ti\text{-}O\text{-}H}$	log $P_{Ti\text{-}O\text{-}H}$	log P_{O2}	log P_{H2O}
	(°C)	(K)	(hr)	(mole/sec)	%	(mole/sec)	%	(moles/sec)	%	Torr	(µg Ti)	(mole/sec)	(mL/sec)	atm			
Ti016	1400	1673	20	1.86E-04	100%	---	0%	---	0%	754	3.5	1.01E-12	25.7313	5.41E-09	-8.27	---	---
Ti034	1400	1673	89.4	1.67E-05	17%	7.37E-05	76%	7.08E-06	7%	747	29.2	1.89E-12	13.6201	1.91E-08	-7.72	-0.77	-1.14
Ti032	1401	1674	91	6.69E-05	68%	2.34E-05	24%	7.38E-06	8%	746	29.3	1.87E-12	13.6727	1.88E-08	-7.73	-0.16	-1.12
Ti050	1402	1675	95	---	0%	1.36E-04	86%	2.31E-05	14%	760	29.4	1.79E-12	21.9078	1.13E-08	-7.95	---	-0.84
Ti033	1400	1673	45	1.68E-05	17%	6.72E-05	67%	1.63E-05	16%	749	30.3	3.90E-12	13.9676	3.84E-08	-7.42	-0.78	-0.79
Ti026	1401	1674	20	1.68E-04	80%	---	0%	4.11E-05	20%	750	31.0	8.99E-12	29.1236	4.24E-08	-7.37	-0.09	-0.71
Ti046	1400	1673	114	2.69E-05	20%	7.40E-05	55%	3.25E-05	24%	750	157.6	8.02E-12	18.5509	5.93E-08	-7.23	-0.70	-0.61
Ti030	1403	1676	42.7	1.68E-05	17%	5.04E-05	51%	3.20E-05	32%	750	49.0	6.66E-12	13.8331	6.62E-08	-7.18	-0.77	-0.49
Ti031	1402	1675	45	4.99E-05	51%	1.66E-05	17%	3.20E-05	32%	742	47.1	6.07E-12	13.8729	6.01E-08	-7.22	-0.30	-0.49
Ti038	1404	1677	43	1.02E-05	6%	1.02E-04	61%	5.54E-05	33%	755	95.1	1.28E-11	23.1474	7.62E-08	-7.12	-1.22	-0.48
Ti047	1402	1675	41	3.70E-05	35%	3.36E-05	32%	3.45E-05	33%	750	58.8	8.31E-12	14.6360	7.81E-08	-7.11	-0.45	-0.48
Ti045	1402	1675	90	3.66E-05	41%	2.33E-05	26%	2.92E-05	33%	742	121.4	7.82E-12	12.5462	8.57E-08	-7.07	-0.39	-0.48
Ti043	1404	1677	68	8.07E-05	62%	6.73E-06	5%	4.23E-05	33%	750	134.0	1.14E-11	18.0924	8.69E-08	-7.06	-0.21	-0.49
Ti022	1401	1674	20	---	0%	1.35E-04	65%	7.26E-05	35%	752	26.1	7.57E-12	28.8054	3.61E-08	-7.44	---	-0.46
Ti015	1399	1672	20	1.36E-04	65%	---	0%	7.38E-05	35%	756	52.8	1.53E-11	28.8875	7.27E-08	-7.14	-0.19	-0.45
Ti039	1403	1676	24	2.71E-05	17%	5.42E-05	34%	7.69E-05	49%	755	76.8	1.86E-11	21.8972	1.17E-07	-6.93	-0.77	-0.31
Ti051	1401	1674	43	---	0%	3.98E-05	45%	4.89E-05	55%	739	38.1	5.14E-12	12.5285	5.63E-08	-7.25	---	-0.26
Ti052	1400	1673	52.7	1.99E-05	22%	1.99E-05	22%	4.89E-05	55%	740	107.4	1.18E-11	12.5117	1.30E-07	-6.89	-0.65	-0.26
Ti042	1402	1675	23	---	0%	6.08E-05	30%	1.42E-04	70%	753	130.8	3.30E-11	28.0655	1.62E-07	-6.79	---	-0.16
Ti041	1402	1675	47	5.39E-05	28%	---	0%	1.42E-04	72%	751	261.8	3.23E-11	27.2237	1.63E-07	-6.79	-0.56	-0.14
Ti023	1401	1674	20	---	0%	5.38E-05	27%	1.43E-04	73%	750	79.2	2.30E-11	27.3623	1.15E-07	-6.94	---	-0.14
Ti044	1402	1675	43	3.32E-05	20%	6.64E-06	4%	1.23E-04	76%	740	207.3	2.80E-11	22.9940	1.67E-07	-6.78	-0.69	-0.12

Run	Temp	Temp	Time	O_2 gas flow rate		Ar gas flow rate		H_2O flow rate		Room P_{total}	[Ti]	Condensate	Cell Flow rate	$P_{Ti\text{-}O\text{-}H}$	log $P_{Ti\text{-}O\text{-}H}$	log P_{O2}	log P_{H2O}
	(°C)	(K)	(hr)	(mole/sec)	%	(mole/sec)	%	(moles/sec)	%	Torr	(µg Ti)	(mole/sec)	(mL/sec)	atm			
Ti074	1301	1574	91	5.78E-05	34%	9.52E-05	57%	1.54E-05	9%	758	19.6	1.25E-12	21.7993	7.40E-09	-8.13	-0.46	-1.04
Ti077	1301	1574	114	---	0%	1.42E-04	90%	1.63E-05	10%	755	18.6	9.46E-13	20.6067	5.93E-09	-8.23	---	-0.99
Ti079	1300	1573	116	5.74E-05	34%	8.44E-05	50%	2.77E-05	16%	753	32.7	1.63E-12	22.0824	9.56E-09	-8.02	-0.47	-0.79
Ti001	1300	1573	168	1.53E-04	81%	---	0%	3.54E-05	19%	754	57.0	1.97E-12	24.486	1.04E-08	-7.98	-0.09	-0.73
Ti004	1300	1573	24	---	0%	1.48E-04	76%	4.62E-05	24%	757	13.8	3.33E-12	25.1155	9.63E-09	-8.02	---	-0.62
Ti017	1298	1571	115	---	0%	1.55E-04	76%	4.77E-05	24%	752	39.5	1.99E-12	26.422	9.72E-09	-8.01	---	-0.63
Ti003	1301	1574	114.5	1.52E-04	76%	---	0%	4.77E-05	24%	748	48.1	2.44E-12	26.1536	1.20E-08	-7.92	-0.12	-0.62
Ti062	1301	1574	94	5.08E-05	25%	1.02E-04	51%	4.77E-05	24%	755	43.0	2.65E-12	26.0075	1.32E-08	-7.88	-0.60	-0.62
Ti063	1301	1574	64	3.37E-05	21%	8.77E-05	55%	3.88E-05	24%	752	23.9	2.16E-12	20.9061	1.34E-08	-7.87	-0.68	-0.62
Ti064	1302	1575	66	1.68E-05	10%	1.08E-04	66%	3.98E-05	24%	750	26.0	2.28E-12	21.5144	1.37E-08	-7.86	-0.99	-0.62
Ti058	1301	1574	71	---	0%	1.35E-04	67%	6.77E-05	33%	752	28.4	2.32E-12	26.4421	1.13E-08	-7.95	---	-0.48
Ti072	1301	1574	46	5.78E-05	34%	5.52E-05	32%	5.88E-05	34%	750	27.6	3.48E-12	22.4808	2.00E-08	-7.70	-0.47	-0.47
Ti073	1301	1574	48	1.69E-05	10%	9.83E-05	56%	6.09E-05	35%	756	29.4	3.55E-12	22.8755	2.01E-08	-7.70	-1.02	-0.46
Ti071	1301	1574	49	1.05E-04	65%	---	0%	5.54E-05	35%	752	24.0	2.84E-12	20.8742	1.76E-08	-7.76	-0.18	-0.46
Ti080	1299	1572	29	8.74E-05	50%	2.69E-05	15%	6.20E-05	35%	750	18.0	3.60E-12	23.0504	2.01E-08	-7.70	-0.30	-0.45
Ti013	1301	1574	20	---	0%	1.18E-04	61%	7.66E-05	39%	753	11.5	3.33E-12	25.3927	1.70E-08	-7.77	---	-0.41
Ti070	1298	1571	49	6.77E-05	35%	---	0%	1.28E-04	65%	755	63.5	7.51E-12	25.4558	3.80E-08	-7.42	-0.46	-0.18
Ti076	1299	1572	43	---	0%	5.19E-05	30%	1.23E-04	70%	752	54.9	7.40E-12	22.8145	4.19E-08	-7.38	---	-0.15

Run	Temp	Temp	Time	O_2 gas flow rate		Ar gas flow rate		H_2O flow rate		Room P_{total}	[Ti]	Condensate	Cell Flow rate	$P_{Ti\text{-}O\text{-}H}$	log $P_{Ti\text{-}O\text{-}H}$	log P_{O2}	log P_{H2O}
	(°C)	(K)	(hr)	(mole/sec)	%	(mole/sec)	%	(moles/sec)	%	Torr	(µg Ti)	(mole/sec)	(mL/sec)	atm			
Ti010	1200	1473	50	---	0%	1.35E-04	100%	---	0%	750	1.2	1.39E-13	16.4765	1.02E-09	-8.99	---	---
Ti075	1200	1473	216	1.15E-04	65%	4.73E-05	27%	1.54E-05	9%	754	9.2	3.14E-13	21.6461	1.75E-09	-8.76	-0.19	-1.06
Ti083	1200	1473	250	6.73E-05	34%	1.01E-04	51%	3.00E-05	15%	750	13.5	7.83E-13	24.2700	3.90E-09	-8.41	-0.47	-0.82
Ti084	1200	1473	240	5.04E-05	32%	5.38E-05	34%	5.23E-05	33%	750	26.3	2.03E-12	19.1759	1.28E-08	-7.89	-0.49	-0.48
Ti055	1198	1471	140	---	0%	1.35E-04	66%	6.92E-05	34%	755	12.0	4.97E-13	24.8659	2.41E-09	-8.62	---	-0.47
Ti068	1200	1473	94	5.89E-05	34%	2.37E-05	14%	9.08E-05	52%	755	23.6	1.57E-12	21.0944	9.01E-09	-8.05	-0.47	-0.28
Ti066	1200	1473	115	2.69E-05	16%	5.38E-05	31%	9.18E-05	53%	750	25.2	3.65E-12	21.1351	2.09E-08	-7.68	-0.81	-0.27
Ti067	1198	1471	118	---	0%	6.75E-05	35%	1.23E-04	65%	753	35.6	1.75E-12	23.2584	9.08E-09	-8.04	---	-0.19

Run	Temp	Temp	Time	O_2 gas flow rate		Ar gas flow rate		H_2O flow rate		Room P_{total}	[Ti]	Condensate	Cell Flow rate	$P_{Ti\text{-}O\text{-}H}$	log $P_{Ti\text{-}O\text{-}H}$	log P_{O2}	log P_{H2O}
	(°C)	(K)	(hr)	(mole/sec)	%	(mole/sec)	%	(moles/sec)	%	Torr	(µg Ti)	(mole/sec)	(mL/sec)	atm			
Ti082	1225	1498	138	6.36E-05	34%	6.09E-05	33%	6.09E-05	33%	754	29.6	1.83E-12	22.9638	9.77E-09	-8.01	-0.46	-0.48
Ti057	1250	1523	144	---	0%	1.35E-04	67%	6.62E-05	33%	754	22.0	8.86E-13	25.3688	4.36E-09	-8.36	---	-0.48
Ti081	1275	1548	119	6.42E-05	34%	6.09E-05	33%	6.17E-05	33%	754	45.4	2.77E-12	23.9154	1.47E-08	-7.83	-0.46	-0.48

Appendix B.—Data for Third Law Method

Temperature	1/T(K)	Delta gef Bent OH	ln Keq	Third Law DH298	Delta gef Linear OH	Third Law DH298
1673	0.000598	-116.792	-15.1676	406369.1228	-75.93136	338008.6359
1674	0.000597	-116.8	-15.2272	407453.6275	-75.93016	339037.7809
1675	0.000597	-116.807	-16.3695	423617.2617	-75.92895	355146.038
1673	0.000598	-116.792	-15.2736	407843.1928	-75.93136	339482.7058
1674	0.000597	-116.8	-15.3613	409319.9401	-75.93016	340904.0934
1673	0.000598	-116.792	-15.2403	407379.9287	-75.93136	339019.4418
1676	0.000597	-116.815	-15.4115	410533.756	-75.92774	342007.138
1675	0.000597	-116.807	-15.5262	411872.8927	-75.92895	343401.669
1677	0.000596	-116.822	-15.292	409124.4252	-75.92654	340542.3955
1675	0.000597	-116.807	-15.2639	408220.1153	-75.92895	339748.8916
1675	0.000597	-116.807	-15.182	407079.7021	-75.92895	338608.4784
1677	0.000596	-116.822	-15.1507	407155.2632	-75.92654	338573.2335
1674	0.000597	-116.8	-16.0984	419578.7535	-75.93016	351162.9069
1672	0.000598	-116.785	-15.3993	409333.8455	-75.93257	341028.7009
1676	0.000597	-116.815	-15.2511	408297.7968	-75.92774	339771.1787
1674	0.000597	-116.8	-16.1254	419955.0686	-75.93016	351539.2219
1673	0.000598	-116.792	-15.2887	408053.3257	-75.93136	339692.8387
1675	0.000597	-116.807	-15.2905	408590.5246	-75.92895	340119.3009
1675	0.000597	-116.807	-15.3191	408988.8831	-75.92895	340517.6594
1674	0.000597	-116.8	-15.6691	413603.7866	-75.93016	345187.9399
1675	0.000597	-116.807	-15.3506	409428.3905	-75.92895	340957.1668
1574	0.000635	-116.054	-16.3317	396394.6267	-76.05076	333429.0053
1574	0.000635	-116.054	-16.6756	400895.1623	-76.05076	337929.5409
1573	0.000636	-116.047	-16.6636	400471.8127	-76.05196	337559.8188
1573	0.000636	-116.047	-16.7208	401219.4366	-76.05196	338307.4427
1573	0.000636	-116.047	-17.027	405224.2235	-76.05196	342312.2296
1571	0.000637	-116.032	-17.0123	404493.631	-76.05437	341688.8401
1574	0.000635	-116.054	-16.8217	402806.0317	-76.05076	339840.4103
1574	0.000635	-116.054	-16.7178	401447.2943	-76.05076	338481.6729
1574	0.000635	-116.054	-16.723	401514.4916	-76.05076	338548.8702
1575	0.000635	-116.062	-16.7008	401491.5834	-76.04955	338472.3172
1574	0.000635	-116.054	-17.2102	407890.5743	-76.05076	344924.9529
1574	0.000635	-116.054	-16.6687	400804.3337	-76.05076	337838.7123
1574	0.000635	-116.054	-16.6681	400796.9787	-76.05076	337831.3574
1574	0.000635	-116.054	-16.807	402614.169	-76.05076	339648.5476
1572	0.000636	-116.039	-16.6883	400527.971	-76.05317	337669.5873
1574	0.000635	-116.054	-16.9685	404727.0739	-76.05076	341761.4525
1571	0.000637	-116.032	-16.6681	399996.7865	-76.05437	337191.9956
1572	0.000636	-116.039	-16.6474	399993.5658	-76.05317	337135.1821
1473	0.000679	-115.301	-17.7622	387368.6802	-76.17256	329731.9574
1473	0.000679	-115.301	-17.4879	384009.4705	-76.17256	326372.7477
1473	0.000679	-115.301	-17.0893	379127.7265	-76.17256	321491.0037
1471	0.00068	-115.286	-18.7652	399086.633	-76.17497	341553.6487
1473	0.000679	-115.301	-17.884	388859.3672	-76.17256	331222.6444
1473	0.000679	-115.301	-17.0664	378847.1262	-76.17256	321210.4033
1471	0.00068	-115.286	-18.0899	390828.475	-76.17497	333295.4907
1498	0.000668	-115.488	-17.3388	388948.1109	-76.14241	330008.8099
1523	0.000657	-115.674	-18.1444	405924.2396	-76.11226	345671.534
1548	0.000646	-115.86	-16.9341	397299.9433	-76.08211	335723.0067

References

1. Jacobson, N., et al., Interactions of water vapor with oxides at elevated temperatures. Journal of Physics and Chemistry of Solids, 2005. 66(2-4): p. 471-478.
2. Meschter, P.J., E.J. Opila, and N.S. Jacobson, Water Vapor Mediated Volatilization of High Temperature Materials, in Annual Reviews of Materials Research, D.M. Lipkin, Editor. 2013, Annual Reviews, Inc.
3. Chase, M.W. and National Institute of Standards and Technology (U.S.), NIST-JANAF thermochemical tables. 4th ed. Journal of physical and chemical reference data Monograph. 1998, Washington, D.C. Woodbury, N.Y.: American Chemical Society; American Institute of Physics for the National Institute of Standards and Technology.
4. Hashimoto, A., The effect of H_2O gas on volatilities of planet-forming major elements: I. Experimental determination of thermodynamic properties of Ca-, Al-, and Si-hydroxide gas molecules and its application to the solar nebula. Geochimica et Cosmochemica Acta, 1992. 56, 511-532.
5. Jacobson, N.S., et al., Thermodynamics of gas phase species in the Si-O-H system. Journal of Chemical Thermodynamics, 2005. 37(10): p. 1130-1137.
6. Plyasunov, A.V., Thermodynamic properties of H4SiO4 in the ideal gas state as evaluated from experimental data. Geochimica et Cosmochemica Acta, 2011. 75(12): p. 3853-65.
7. Opila, E.J., et al., Theoretical and experimental investigation of the thermochemistry of $CrO_2(OH)_2(g)$. Journal of Physical Chemistry A, 2007. 111(10): p. 1971-1980.
8. Kauffman, J.W., R.H. Hauge, and J.L. Margrave, Studies of Reactions of Atomic and Diatomic Cr, Mn, Fe, Co, Ni, Cu, and Zn with Molecular Water at 15-K. Journal of Physical Chemistry, 1985. 89(16): p. 3541-3547.
9. Zhou, M.F., et al., Reactions of group IV metal atoms with water molecules. Matrix isolation FTIR and theoretical studies. Journal of the American Chemical Society, 2000. 122(43): p. 10680-10688.
10. Wang, X.F. and L. Andrews, Infrared spectra and structures for group 4 dihydroxide and tetrahydroxide molecules. Journal of Physical Chemistry A, 2005. 109(47): p. 10689-10701.
11. Shao, L.M., et al., Reactions of titanium oxides with water molecules. A matrix isolation FTIR and density functional study. Chemical Physics Letters, 2001. 343(1-2): p. 178-184.
12. Ueno, S., et al., Anistropic Behavior of Water Vapor Corrosion of Rutile TiO2 at High Temperature. Materials Transactions--JIM, 2004. 45(2): p. 281-283.
13. Ayers, J.C. and E.B. Watson, Rutile Solubility and Mobility in Supercritical Aqueous Fluids. Contributions to Mineralogy and Petrology, 1993. 114(3): p. 321-330.
14. Glemser, O. and H.G. Wendlandt, Gaseous Hydroxides, in Advances in Inorganic Chemistry and Radiochemistry, H.J. Emeléus and A.G. Sharpe, Editors. 1963, Academic Press. p. 215-258.
15. Belton, G.R. and R.L. McCarron, The Volatilization of Tungsten in the Presence of Water Vapor. The Journal of Physical Chemistry, 1964. 68(7): p. 1852-1856.
16. Merten, U. and W.E. Bell, The Transpiration Method, in The Characterization of High Temperature Vapors, J.L. Margrave, Editor. 1963, John Wiley & Sons: New York. p. 91-114.
17. Anzelmo, J.A. and J.R. Lindsay, X-Ray-Fluorescence Spectrometric Analysis of Geologic Materials. Part 2. Applications. Journal of Chemical Education, 1987. 64(9): p. A200-A204.
18. Drowart, J. and P. Goldfinger, Investigation of Inorganic Systems at High Temperature by Mass Spectrometry. Angewandte Chemie-International Edition, 1967. 6(7): p. 581-648.
19. Lewis, G.N. and M. Randall, Thermodynamics, Revised by K.S. Pitzer and L. Brewer, Second Edition, McGraw-Hill, New York, 1961, pp. 419-448.
20. Frisch, M.J., et al., Gaussian 09, Revision B. 01. 2010, Wallingford, CT: Gaussian, Inc.
21. Pitzer, K.S. and W.D. Gwinn, Energy Levels and Thermodynamic Functions for Molecules with Internal Rotation I. Rigid Frame with Attached Tops. Journal of Chemical Physics 1942. 10, pp. 428-440.

22. Chekhovskoi, D.V., et al., IVTANTHERMO database on thermodynamic properties of individual substances, in NIST special database 5. 1993, CRC Press: Boca Raton.
23. Bauschlicher, C. Theoretical Studies of the First Transition Row Oxides and Sulfides. Theoretica Chimica Acta (1995) 92: 183-198.
24. Feller, D., The role of databases in support of computational chemistry calculations. Journal of Computational Chemistry, 1996. 17(13): p. 1571-1586.
25. Schuchardt, K.L., et al., Basis set exchange: A community database for computational sciences. Journal of Chemical Information and Modeling, 2007. 47(3): p. 1045-1052.
26. Opila, E.J. and R.A. Golden, unpublished work.
27. Geiger, G.H. and D.R. Poirier, Transport Phenomena in Metallurgy, Addison-Wesley Publishing Co., Reading, MA, 1973, p. 532.
28. Welty, J., C.E. Wicks, G.L. Rorrer, R.E. Wilson, Fundamentals of Momentum, Heat and Mass Transfer, 5th Edition, Wiley, 2008.
29. Ueno, S., et al., Development of Oxide-Based EBC for Silicon Nitride. Int. J. Appl. Ceram. Tech., 2004, 1 [4], 362-373.
30. Svehla, R.A., Estimated Viscosities and Thermal Conductivities of Gases at High Temperatures, NASA TR-R-132, 1962.
31. Opila, E.J. and D.L. Myers, Alumina Volatility at Elevated Temperatures. J. Am. Ceram. Soc. 2004, 87 [9], 1701-1705.
32. Opila, E.J. and R.E. Hann, Jr., Paralinear Oxidation of CVD SiC in Water Vapor. J. Am. Ceram. Soc. 1997, 80 [1], 197-205.